Climate Dynamics
https://doi.org/10.1007/s00382-019-05031-5

An inter-basin teleconnection from the North Atlantic to the subarctic North Pacific at multidecadal time scales

Zhanqiu Gong[1] · Cheng Sun[1,2] · Jianping Li[3] · Juan Feng[1] · Fei Xie[1] · Ruiqiang Ding[4] · Yun Yang[1] · Jiaqing Xue[5]

Received: 25 April 2019 / Accepted: 26 October 2019

Abstract
Observational evidence suggests that the sub-arctic North Pacific (SANP; 45°–60° N, 155° E–165° W) sea surface temperature (SST) shows pronounced multidecadal variability, which cannot be explained by the Pacific Decadal Oscillation (PDO). Here, we find that the SANP SST multidecadal variability is closely linked to the remote Atlantic Multidecadal Oscillation (AMO), indicating a multidecadal inter-basin teleconnection. The teleconnection can be well reproduced in a set of Atlantic Pacemaker experiments. An atmospheric bridge mechanism for the teleconnection is proposed by analyzing both observations and simulation data. The AMO warm phase generates anomalous ascent and upper-level divergence over the North Atlantic. The upper-level outflows converge towards the subarctic North Pacific, leading to compensating subsidence along with anomalous high pressure there. The enhanced adiabatic descent causes anomalous warming and moistening of the lower troposphere above the SANP basin and increases the downwelling longwave radiation. The warming of the SANP SST is further induced and amplified due to water vapor-longwave radiation-SST positive feedback. The anomalous high also weakens the climatological cyclonic flow of Aleutian low and suppresses the turbulent heat release from ocean to atmosphere, contributing to the SANP SST warming. Our findings suggest that the AMO plays a crucial role in the subarctic North Pacific SST multidecadal variability.

Keywords Inter-basin teleconnection · Atlantic Multidecadal Oscillation · Sub-arctic North Pacific · Multidecadal variability

1 Introduction

The observed climate records show that global mean sea surface temperature (SST) has been increasing since the records began, and previous studies have indicated that the increase in greenhouse gas concentrations has led to the century-long warming trend. However, the global mean SST does not increase monotonously, and we can see both an interdecadal acceleration and a slowdown of the SST warming (Trenberth and Fasullo 2013; Kosaka and Xie 2013; Zhang 2016). These trends may be due to the interdecadal SST variability, which is superimposed on secular warming and modulates the warming trend (Timmermann et al. 1998).

Electronic supplementary material The online version of this article (https://doi.org/10.1007/s00382-019-05031-5) contains supplementary material, which is available to authorized users.

✉ Cheng Sun
scheng@bnu.edu.cn

1 College of Global Change and Earth System Science (GCESS), Beijing Normal University, Beijing 100875, China

2 State Key Laboratory of Satellite Ocean Environment Dynamics, Second Institute of Oceanography, Ministry of Natural Resources, Hangzhou, China

3 Key Laboratory of Physical Oceanography-Institute for Advanced Ocean Studies, Ocean University of China and Qingdao National Laboratory for Marine Science and Technology, Qingdao 266100, China

4 State Key Laboratory of Numerical Modeling for Atmospheric Sciences and Geophysical Fluid Dynamics, Institute of Atmospheric Physics, Chinese Academy of Sciences, Beijing, China

5 Key Laboratory of Meteorological Disaster of Ministry of Education/ Collaborative Innovation Center on Forecast and Evaluation of Meteorological Disasters/ Institute for Climate and Application Research (ICAR), Nanjing University of Information Science and Technology, Nanjing 210044, China

Published online: 26 November 2019

Hence, it is necessary to understand the interdecadal SST variability and the associated spatial patterns. The interdecadal SST variability is most pronounced in the North Pacific and North Atlantic oceans (Li et al. 2009), which are dominated by two well-known interdecadal SST modes: the Pacific Decadal Oscillation (PDO; Zhang et al. 1997; Mantua et al. 1997) and the Atlantic Multidecadal Oscillation (AMO; Kerr 2000).

The PDO is a robust pattern of North Pacific interdecadal SST variability characterized by a spatially coherent SST pattern centered over the extratropical North Pacific Ocean, with its warm/cool phase lasting approximately 20–30 years. The PDO index can be derived from the leading empirical orthogonal function (EOF) of SST anomalies in the North Pacific poleward of 20° N (Zhang et al. 1997; Mantua et al. 1997). Previous studies indicate that the PDO plays a crucial role in continental climate variability over coastal regions extending from the extratropical North Pacific to the Arctic region, such as North America (Bromirski et al. 2011) and Alaska (Hartmann and Wendler 2005). The AMO is the dominant mode of multidecadal SST variability in the North Atlantic (Enfield et al. 2001; Kerr 2000). The AMO exhibits an oscillation over a period of approximately 50–70 years between warm and cold phases. Many studies based on global climate model simulations have shown that changes in northward ocean heat transport associated with the Atlantic meridional overturning circulation (AMOC) cause the phase changes of the AMO (Delworth and Mann 2000; Knight et al. 2005; O'Reilly et al. 2017; Sun et al. 2015; Zhang and Wang 2013; Zhang et al. 2013). As one of the most important internal climate modes, the AMO has wide impacts on the climate around the North Atlantic region (Enfield et al. 2001; McCabe et al. 2004; Sutton and Dong 2012; Sutton and Hodson 2005) and in remote regions (Li and Bates 2007; Lu et al. 2006; Sun et al. 2015, 2017) such as the East Asia and Indian oceans.

Inter-basin interactions at decadal time scales have received considerable attention in recent years as many studies have suggested a strong SST teleconnection from North Atlantic to Pacific and an SST dipole between the North and South Atlantic arises at multidecadal time scales (Lopez et al. 2016). This topic remains understudied and is important for understanding the origin of regional decadal climate variability and predictability. Previous studies have proposed two main mechanisms to explain the remote AMO impacts on the North Pacific: an atmospheric bridge and an oceanic bridge (Liu and Alexander 2007). Various studies of coupled general circulation models (CGCMs) and water-hosing experiments (Stouffer et al. 2006; Timmermann et al. 2007; Wu et al. 2008) have tended to demonstrate that both atmospheric and oceanic bridges will serve as the inter-basin teleconnection between the North Atlantic and North Pacific. The atmospheric bridge indicated that the AMO warm phase forces the reduction of the midlatitude meridional SST gradients and causes northward shifts of the westerlies over the North Pacific. This weakens the Aleutian low and further leads to a warm SST over the North Pacific (Deser et al. 1999; Wu et al. 2008; Zhang and Delworth 2007). Many modeling studies found a resonance over the North Atlantic and the North Pacific, suggesting that the variation of the SST in the North Atlantic associated with the AMO acts as a major driver of the SST changes over the North Pacific at multidecadal time scales, and some of them also focused on the tropical teleconnection and the role of tropical North Atlantic warming/cooling in modulating the Pacific climate (Li et al. 2015; McGregor et al. 2014; Ruprich-Robert et al. 2017). Okumura et al. (2009) and Hu and Meehl (2005) emphasized the role of oceanic teleconnection, showing that the Arctic Ocean is a key region connecting the North Atlantic and North Pacific through freshwater heat and salinity transmission. These modeling results mostly indicated that the AMO will cause an extratropical North Pacific response that projects well onto a PDO-like pattern, suggesting a significant inter-basin teleconnection between the North Atlantic and North Pacific despite different mechanisms.

The results mentioned above are mostly based on model simulations. Although these modeling studies suggested a strong response of the PDO to the AMO, considerable discrepancies exist between the model simulations and the observations. Observational studies demonstrated that the simultaneous correlation between the PDO and the AMO is weak, almost approximately − 0.1. Strong correlations can be observed only when the PDO leads or lags the AMO by 10–20 years, and this two-way lead–lag correlation provides little evidence for the causality relationship (d'Orgeville and Peltier 2007; Hetzinger et al. 2011; Wu et al. 2011). The discrepancy between the observations and the simulations may be due to the models' biases and uncertainties in simulating the atmospheric and oceanic inter-basin teleconnection (Kushnir et al. 2002; Lyu and Yu 2017; Richter et al. 2014). The uncertainties also stress that more observational studies are needed to further confirm whether a strong teleconnection exists from the North Atlantic to the extratropical North Pacific. On the other hand, the PDO, defined as the first leading EOF mode of extratropical North Pacific SST anomalies, only explains approximately 30% of the total variance of the North Pacific SST variability. This indicates that the SST variations over the North Pacific basin also exhibit regional-scale features unexplained by the basin-scale coherent PDO mode. Therefore, it is necessary to reexamine the impacts of the AMO from the perspective of the regional-scale SST variability over the extratropical North Pacific.

In this study, we perform statistical analyses on observed data sets and a suite of Atlantic Pacemaker experiments to investigate the connection between the North Atlantic and the extratropical North Pacific SST variability, finding a strong covariability between the North Atlantic and the sub-arctic North Pacific (SANP; 45°–60° N, 155° E–165° W) at decadal time scales. An atmospheric bridge mechanism is proposed to explain the teleconnection from the AMO to the subarctic North Pacific, and the thermodynamic processes involved are analyzed. Our results highlight the remote influence of the AMO on subarctic North Pacific SST interdecadal variability. Meanwhile, the SANP region is known as one of the world's most biologically productive marine regions, supporting a large oceanic fishery for both subsistence and commercial use (Hunt et al. 2011), and the marine ecosystem is vulnerable to long-term anomalies of ocean temperatures (Danielson et al. 2011; Hunt et al. 2002; Mueter and Litzow 2008; Stabeno et al. 2012). Therefore, our findings may also have implications for better understanding the drivers of marine ecosystem changes over the SANP region.

The paper is constructed as follows. A brief introduction to the observational data sets and the experiment we performed is given in the next section. The results are presented in Sect. 3. The paper concludes with a summary and discussion.

2 Data and methodology

2.1 Data

The global observational SST data sets used in this study include the Kaplan SST data set (Kaplan et al. 1998), the Hadley Centre Sea Ice and Sea Surface Temperature (HadISST) data set (Rayner et al. 2003), the Centennial in situ Observation-Based Estimates (COBE) SST data set (Ishii et al. 2005) and the Extended Reconstruction SST version 3 (ERSST v3b) data set (Smith et al. 2008). Atmospheric data sets from the ECMWF Atmospheric Reanalysis of the twentieth Century (ERA-20C) data set (Stickler et al. 2014) include geopotential height, wind, air temperature, and water vapor.

The AMO index is defined as the area-weighted average of SST anomalies over the North Atlantic region (0°–60° N, 80° W–0°), and the subarctic North Pacific SST index is defined for the region (45°–60° N, 155° E–165° W) in the same way. The PDO index we used in this paper is downloaded from the Japan Meteorological Agency and is defined as the projections of monthly mean SST anomalies which subtracts globally averaged monthly mean SST anomalies onto their first EOF vectors in the North Pacific (north of 20° N).

2.2 Statistical methods

We confine our analysis to the post-1900 period for the data sets because uncertainties in surface observations prior to 1900 are relatively large and the data before 1900 are deemed less reliable (Folland et al. 2001). To better isolate and highlight the signal of decadal to multidecadal variability, we tend to remove the centennial scale trends. Various methods have been applied to separating internally natural variability (Enfield and Cid-Serrano 2009; Sutton and Dong 2012; Trenberth and Shea 2006), including removal of linear trend, removal of a quadratic trend, removal of the global mean SST from the North Atlantic SST, referred to as TS method, and the other removal of the global mean SST outside the North Atlantic, referred to as SD method. Several other studies use more sophisticated methods based on the large ensemble simulation results from CMIP5 models to identify the externally forced component of the historical global SST. For example, Frankcombe et al. (2015) and Frankcombe and England (2018) used scaling methods on the forced signal obtained from ensembles of climate models to extract the natural variability. In this study, we use the removal of linear trend to remove the long-term linear trend in the variables for the post-1900 period. Here we also perform other two methods to further test the robustness of the main findings presented in our study. Both removal of a quadratic trend (a least squares quadratic fit of the secular warming trend) (Enfield and Cid-Serrano 2009) and removal of the global mean SST outside the North Atlantic (regarded as the forced SST) as in Sutton and Dong (2012), which is referred to as SD method, give similar results.

A two-tailed Student's t test was used to determine the statistical significance of the linear regression and correlation between two autocorrelated time series. We use the effective number of degrees of freedom, N^{eff}, which is given by the following approximation:

$$\frac{1}{N^{eff}} \approx \frac{1}{N} + \frac{2}{N}\sum_{j=1}^{N}\frac{N-j}{N}\rho_{XX}(j)\rho_{YY}(j) \tag{1}$$

where N is the sample size and $\rho_{XX}(j)$ and $\rho_{YY}(j)$ are the autocorrelations of two sampled time series X and Y, respectively, at time lag j (Li et al. 2013; Sun et al. 2016).

2.3 Model and experiments

The model which we used is the International Centre for Theoretical Physics AGCM (ICTPAGCM, version 41) coupled to a slab ocean thermodynamic mixed-layer model (SOM). The ICTPAGCM is intermediate, contains eight vertical levels and adopts a horizontal resolution of T30 (3.75°×3.75° grid). In the SOM, the depth (d_o) of the mixed layer is constant throughout the whole simulation period, varying between 60 m (d_{omax}) in the extratropics and 40 m (d_{omin}) in the tropics. The climatological annual-averaged mixed layer depth is geographically-varying, generally shallow in the tropics and deep in mid-high latitudes. Besides, a heat flux correction is applied to climatological SST for the SOM and the mixed-layer temperature variation is derived from the integration of the net heat flux into the ocean (the sum of surface shortwave and longwave radiation and sensible and latent heat flux; all fluxes anomalies are defined as positive downward; Kucharski et al. 2016; Sun et al. 2017).

To examine the effects of Atlantic SST variability on the atmospheric circulation over other ocean basins, an experiment referred to as ATL_VARMIX is performed. In the ATL_VARMIX experiment, the ICTPAGCM is coupled with the SOM in the Indo-Pacific region, while raw observational monthly-varying SSTs from the HadISST data prescribed in the Atlantic basin (Atlantic Pacemaker experiment). The Atlantic basin we referred in this experiment is the entire Atlantic basin (60° S–60° N, 70° W–10° E) and the other basins out of the Atlantic are the Indo-Pacific region. The mixed layer is used in the whole Indo-Pacific region. Thus, a buffer zone is set for preventing instability in the transition region between the slab ocean (Indo-Pacific) and the prescribed-SST (Atlantic) regions with a spatial range of 7.5°, in which the SST is calculated from the weighted average of the modelled and prescribed SSTs. The weighting values are one in the prescribed-SST domain and linearly reduced to zero in the buffer zone. The simulations of the ATL_VARMIX experiment are integrated from 1872 to 2013 and contain five ensemble members generated by restarting the model with small initial perturbations. The first 28 years of all simulations are taken as spin up and the results of the rest of the period from 1900 to 2013 are analyzed. The ATL_VARMIX experiment considers the combined effects of Atlantic SST variability and atmosphere–ocean coupling over the Indo-Pacific region. This experiment can produce a similar level of decadal variability of atmospheric circulation and SST over the SANP region in comparison with the observation (Fig. S2).

3 Results

3.1 Connection between the North Atlantic and the subarctic North Pacific

Previous modeling studies found that the decadal variation in SSTs in the extratropical North Pacific exhibits a sympathetic response to the AMO SST forcings, showing that the extratropical North Pacific SST warming is a byproduct of the North Atlantic SST warming (Hetzinger et al. 2011; Ruprich-Robert et al. 2017; Wu et al. 2008). The simulation results of the previous modeling studies also showed that the most significant correlations exist at the midlatitude of the North Pacific, resembling a PDO-like pattern.

First, we examine the observed link of SST variability between the North Atlantic and the extratropical North Pacific at decadal time scales. Here, we use four different observational data sets to further examine the correlation between the AMO and the extratropical North Pacific SSTs. Figure 1 shows the correlation maps between the AMO index and the 11-year running mean SSTs north of 25° N for the detrended observational data sets. Positive correlations can be found over almost the whole extratropical North Pacific, suggesting a coherent covariability of SSTs between the AMO and the extratropical North Pacific SST at decadal time scales, consistent with the results of the mentioned studies to some extent. Although there are a few regional-scale differences among the four observational data sets, the observed correlations are consistent and largely significant at the 99% confidence level at decadal time scales over the subarctic North Pacific (SANP; 45°–60° N, 155° E–165° W). In contrast to previous modeling studies that found a strong coherence between the AMO and midlatitude North Pacific SST, observational results show that the positive correlations are strongest and most significant over the SANP region, while over other parts of the basin, the positive correlations are weak. The results of Kaplan SST and HadISST data sets show that positive correlations are not largely significant but the correlation coefficients remain above 0.7. This finding demonstrates that the remote AMO is highly correlated to the variability of the SANP SST at decadal time scales and the spatial pattern of the AMO-SST correlations over the extratropical North Pacific is unlikely to resemble the PDO-like pattern in observations.

To describe the variability of the SANP SST, we take the indices which are calculated from the area-weighted average of SST anomalies over the SANP region as the SANP SST index. Figure 2 shows the normalized time series of SANP SST indices for 1900–2015 derived from observations (COBE, HadISST, Kaplan and ERSST data sets). The SANP SST indices show a warming trend for 1900–2015 (Fig. 2a). The SANP SST indices after removing the linear trends show pronounced multidecadal variability (Fig. 2b). All four data sets show the same amplitude of SANP SST variability. The time scale of the SANP SST is approximately 40–50 years, with changes of sign in reverse polarity in the 1920s and 1960s and in approximately 2000. The AMO index has similar time scales (Enfield et al. 2001; Schlesinger and Ramankutty 1994), indicating that the AMO and SANP SST are closely connected in spectral characteristics. Although there exist some small differences in the SANP SST indices of different data sets, the decadal seesaws of SANP SST indices are similar; thus, we will use the ERSST data in the following paragraphs.

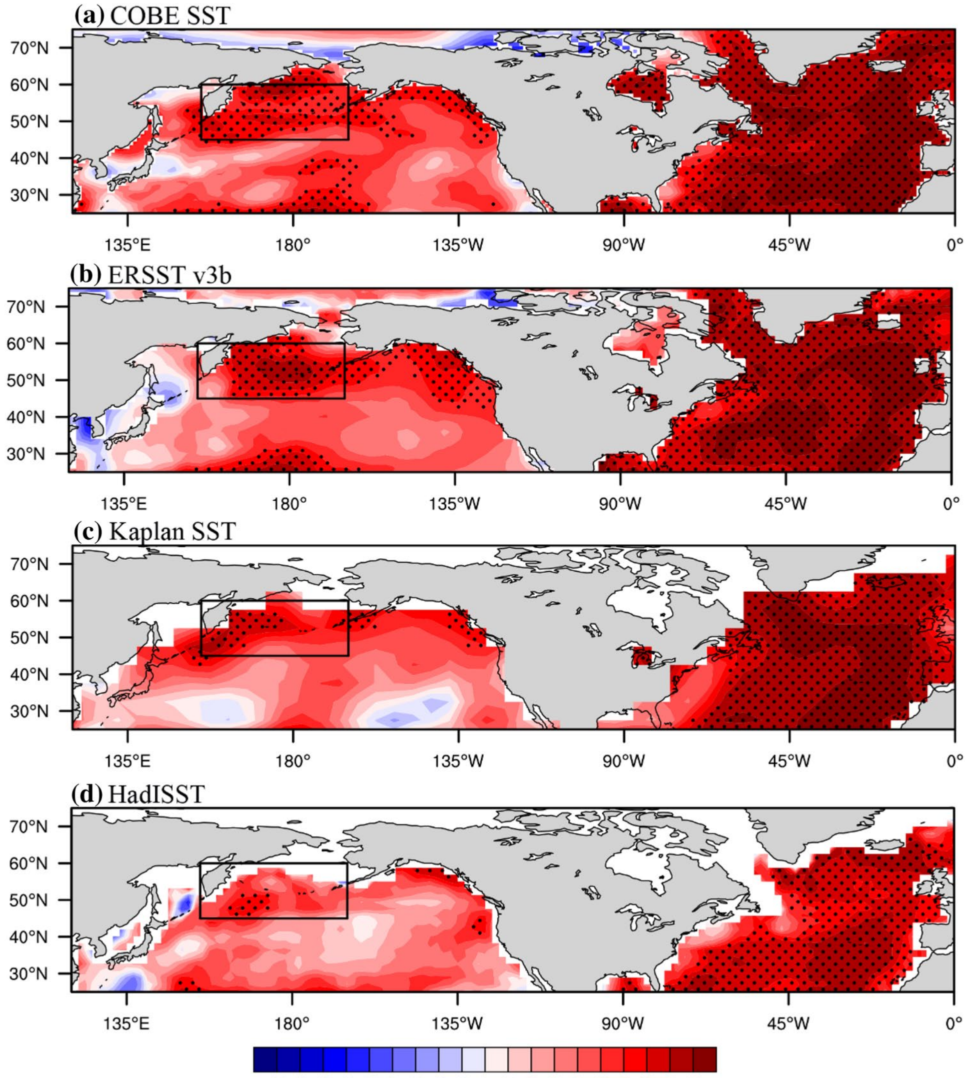

Fig. 1 **a** Correlation map between the AMO index and global SSTs north of 25° N for 1900–2015 based on the COBE SST data set. **b**–**d** As in **a**, but for the results based on the data from the ERSST data, Kaplan SST data and HadISST data. In **a**–**d**, the long-term linear trends in the SST data sets were removed before the correlation analysis, and dots indicate the correlation coefficients significant at the 99% confidence level

The connections among the AMO, PDO and SANP SST decadal variability are further analyzed. Figure 3 shows the normalized time series of the annual mean of the AMO, PDO and SANP SST index for 1900–2015 derived from the ERSST data set. The time series of the AMO (Fig. 3a, blue lines) and the PDO index (Fig. 3b) has a weak simultaneous correlation, almost close to 0 ($r=0.03$), in line with Wu et al. (2011). The spatial pattern of SSTs that we found between the extratropical North Pacific and the AMO is not a PDO-like pattern and can correspond to the weak simultaneous correlation. The correlation between the PDO index and the SANP SST index is also quite weak ($r=-0.08$). Although the PDO is the first leading EOF mode of extratropical North Pacific SST variability, it is not able to fully explain the whole extratropical North Pacific SST decadal variability. The reason why the SANP SST is unlikely to be interpreted by the PDO is that it has regional SST variability at multidecadal time scales. In fact, the SANP SST decadal variability is closely related to the AMO. Highly positive correlation coefficients are observed between the AMO and the SANP SST index at zero lag based on both unfiltered ($r=0.43$, significant at the 95% confidence level) and 11-year running mean ($r=0.86$, significant at the 95% confidence level) data. Both SD method and removal of a quadratic trend are tested using the correlation between the AMO and the SANP SST multidecadal variability. For comparison we use SST from COBE SST (Fig. S1a, b) and ERSST v3b (Fig. S1c, d) between 1900 and 2010. The results show that the SANP SST multidecadal variability and the AMO are highly correlated with correlation coefficients ranging from 0.65 to 0.88, which is qualitatively consistent with the result of the removal of linear trend. The highly positive correlation with the AMO further suggests that the observed AMO–SANP SST connection is strong and robust. In the following analyses, we focus on

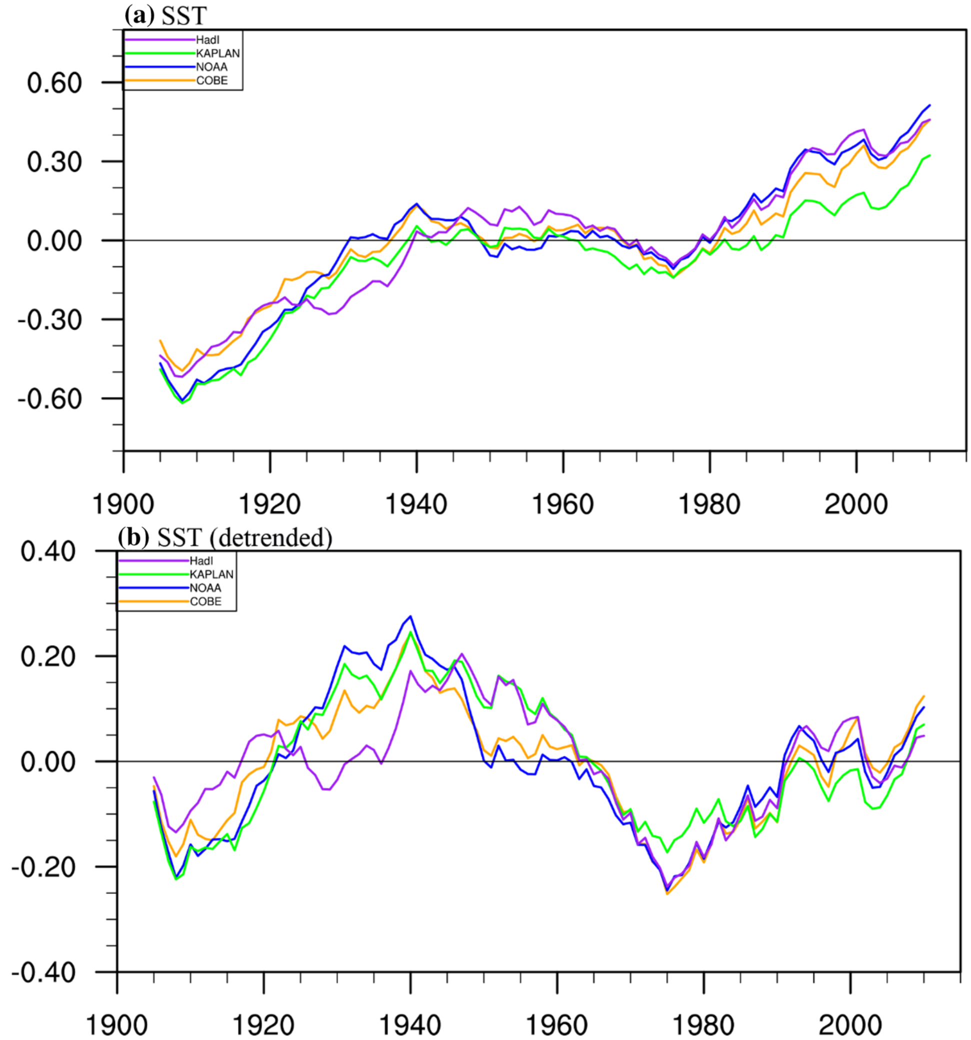

Fig. 2 **a** Time series of the normalized subarctic North Pacific SST anomalies (K) 11-year running average indices for 1900–2015 from observations (HadISST, Kaplan, ERSST and COBE data sets). **b** As in **a**, but for the time series after removing the long-term linear trend

the physical mechanisms of the strong teleconnection from the AMO to the SANP.

3.2 Thermodynamic processes

The SANP SST decadal variability and its connection to the AMO are reasonably well reproduced in the ATL_VARMIX experiment (Atlantic Pacemaker experiment: AGCM coupled to the mixed-layer slab ocean model in the Pacific, whereas observational SSTs are prescribed in the Atlantic; see Model and experiments). In this experiment, high and significant positive correlations (above 0.8) exist over the subarctic North Pacific region in the correlation map of SST with the AMO index (Fig. 4a), consistent with the observational results. Although the positive correlations of midlatitude SSTs with the AMO in the model simulations are stronger and more significant than that in the observations (Fig. 1), the correlations are still weaker than those between the SANP SST and the AMO. The regression pattern of the decadal SST anomalies onto the AMO index is also most pronounced over the SANP region, while over other parts of the basin, the SST anomalies are weaker, and the simulated amplitude of warm SST anomalies is approximately 0.1 K in association with the AMO. This finding further suggests that the ATL_VARMIX experiment reproduces the observed significant coherence between the AMO and the SANP SST decadal variability.

The mechanisms responsible for the SANP SST decadal variability are further investigated by using the ATL_VARMIX simulations. As in ATL_VARMIX experiment, SSTs outside the Atlantic basin are forced only by the surface energy exchanges between the atmosphere and ocean. Wu et al. (2008) also noted that surface heat flux is associated with the North Pacific response to the North Atlantic, which indicates that the thermodynamic process may play a major role. Therefore, a surface heat budget analysis based on the different heat fluxes is performed by examining correlations and regressions of the different surface heat flux components (Fig. 5) onto the AMO index in our studies. Here we define all the heat fluxes anomalies are positive downward in

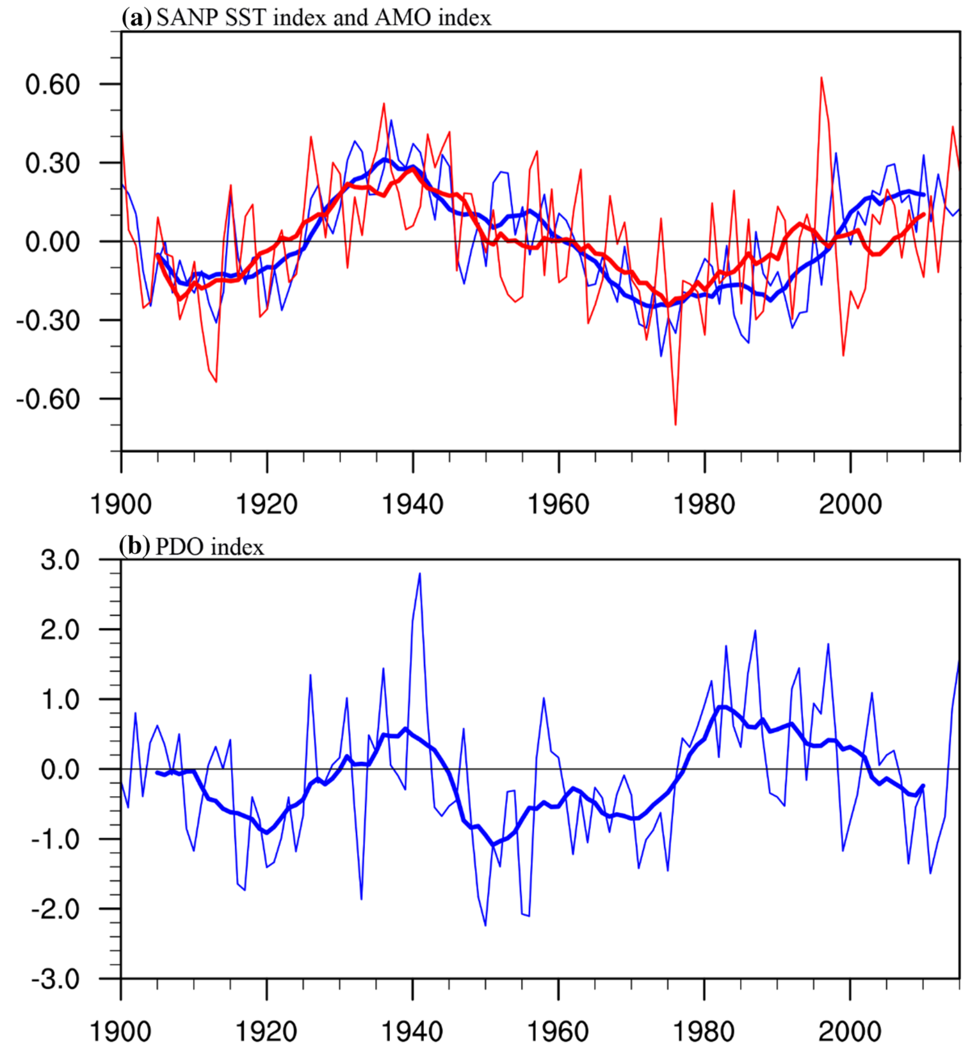

Fig. 3 **a** Time series of the normalized subarctic North Pacific SST index (red lines) and AMO index (K) (blue lines) for 1900–2015 (thin lines) and 11-year running averages (thick lines) derived from the ERSST v3b data set. **b** Time series of the normalized PDO index for 1900–2015 (thin line) and 11-year running averages (thick line). The long-term linear trends were removed in **a** and **b**

order to better discuss the low-level thermodynamic process over the SANP region that leads to the formation of SST anomalies. The spatial patterns of anomalous turbulent heat flux (sensible plus latent heat flux), longwave radiation and total radiation (longwave plus shortwave radiation) all show positive correlations with the AMO over the SANP region while the turbulent heat flux anomalies are not significant (Fig. 5a–c). The regression results are similar with that of correlations but the total radiation anomalies show less significant in the SANP region (Fig. 5d–f).

The longwave radiation anomalies show strong and significant positive correlations with the AMO over the SANP region (Fig. 5c). The shortwave radiation anomalies show a similar spatial pattern with the longwave radiation but with an opposite sign and not as statistically significant as the longwave radiation (Fig. S3). The inverse relationship between shortwave and longwave radiations may suggest a role of cloudiness. The cloudiness over the SANP region shows a weak and statistically insignificant increase associated with the warm AMO phase (Fig. S4a), which probably arises from low-level cloud increase due to the anomalous subsiding motion and increased water vapor trapped near the surface (Fig. 7b). Previous studies have also indicated that high pressure anomalies may favour an increase in cloudiness in the lower level of the atmosphere over the extratropical regions (Clement et al. 2009; Ding et al. 2017). Although the cloudiness gives rise to an offset effect of the shortwave radiation on the longwave radiation, the total radiation (shortwave plus longwave) is still dominated by the longwave radiation and shows a consistent sign with the longwave radiation. The total radiation anomalies show positive correlations with the AMO (Fig. 5b) but the correlation coefficients are smaller than the results of the longwave radiation anomalies over the SANP region. Since the cloudiness has an opposite effect on shortwave and longwave radiations, the role of cloudiness in the total radiation anomaly is minor and negligible. This may indicate that the increased total radiation anomalies are probably largely influenced by the water vapor, and we will further discuss this effect in the following parts.

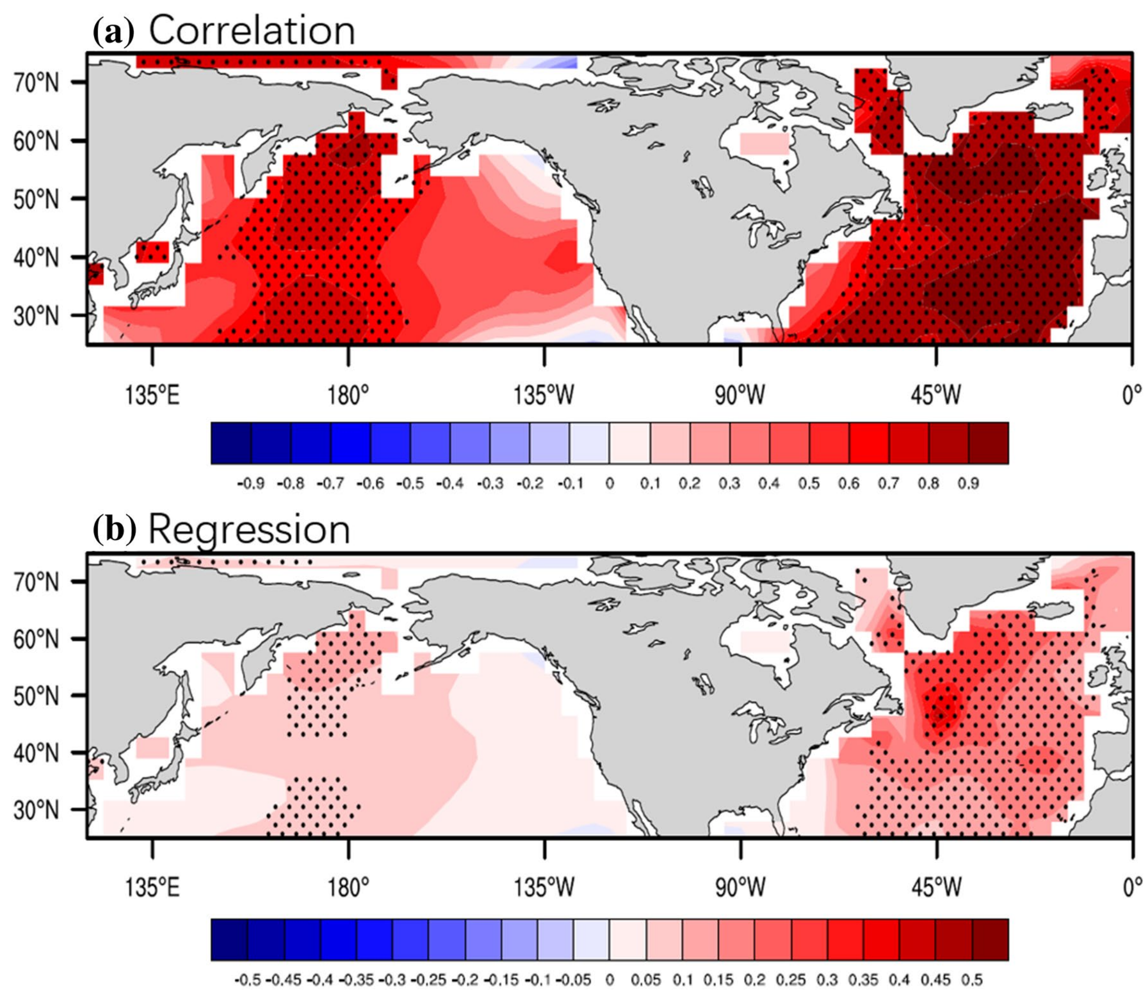

Fig. 4 **a** Correlation map between the decadally filtered AMO index and global SSTs (K) north of 25° N for 1900–2013 in the ATL_VARMIX experiment. **b** As in **a**, but for the regression map. The long-term linear trends for 1900–2013 were removed before the analysis. Dotted shading in **a** and **b** indicates the correlation and regression coefficients significant at the 99% confidence level

It is known that the climatological turbulent heat flux is usually released from ocean to atmosphere. Figure 5a shows that the turbulent heat flux anomalies associated with the AMO are positive but not significant over the SANP region, which corresponds to a decrease of the climatological upward turbulent heat flux in response to the remote AMO. The spatial pattern of the regression is almost same (Fig. 5d). The anomalous turbulent heat flux may also play a role in warming up the SANP SST although it is not that significantly correlated with the AMO. This may be closely related to the variations of atmospheric circulation. The anomalous high pressure weakens the Aleutian low, which further leads to the reduction of low-level cyclonic flow and decrease of evaporation, and prevents the loss of the turbulent heat flux from ocean to atmosphere, leading to the warming of SANP SST. Peings and Magnusdottir (2016) and Sun et al. (2017) also noted that the presence of significant high pressure anomalies in the North Pacific (weakening of the Aleutian Low) in response to the AMO forcing. Besides, enhanced adiabatic descent forced by the accompanied anomalous high induces low-level air warming and moistening, which is also not favorable for the sensible and latent heat release from ocean to atmosphere. Thus, the anomalous turbulent heat flux over the SANP region is not that significantly correlated with the AMO index but still plays a role in warming up the SANP SST during the thermodynamic process.

The lagged correlations between anomalous heat flux components over the SANP region and the AMO index, exhibiting a nearly symmetrical distribution about the zero lag (Fig. 6a) and the surface longwave radiation anomalies show a significant positive correlation at the zero lag, while the correlation at the zero lag of the anomalous total heat flux and turbulent heat flux are weaker, which is consistent with the spatial pattern. We can see that the longwave radiation anomalies take large part in the heat flux components

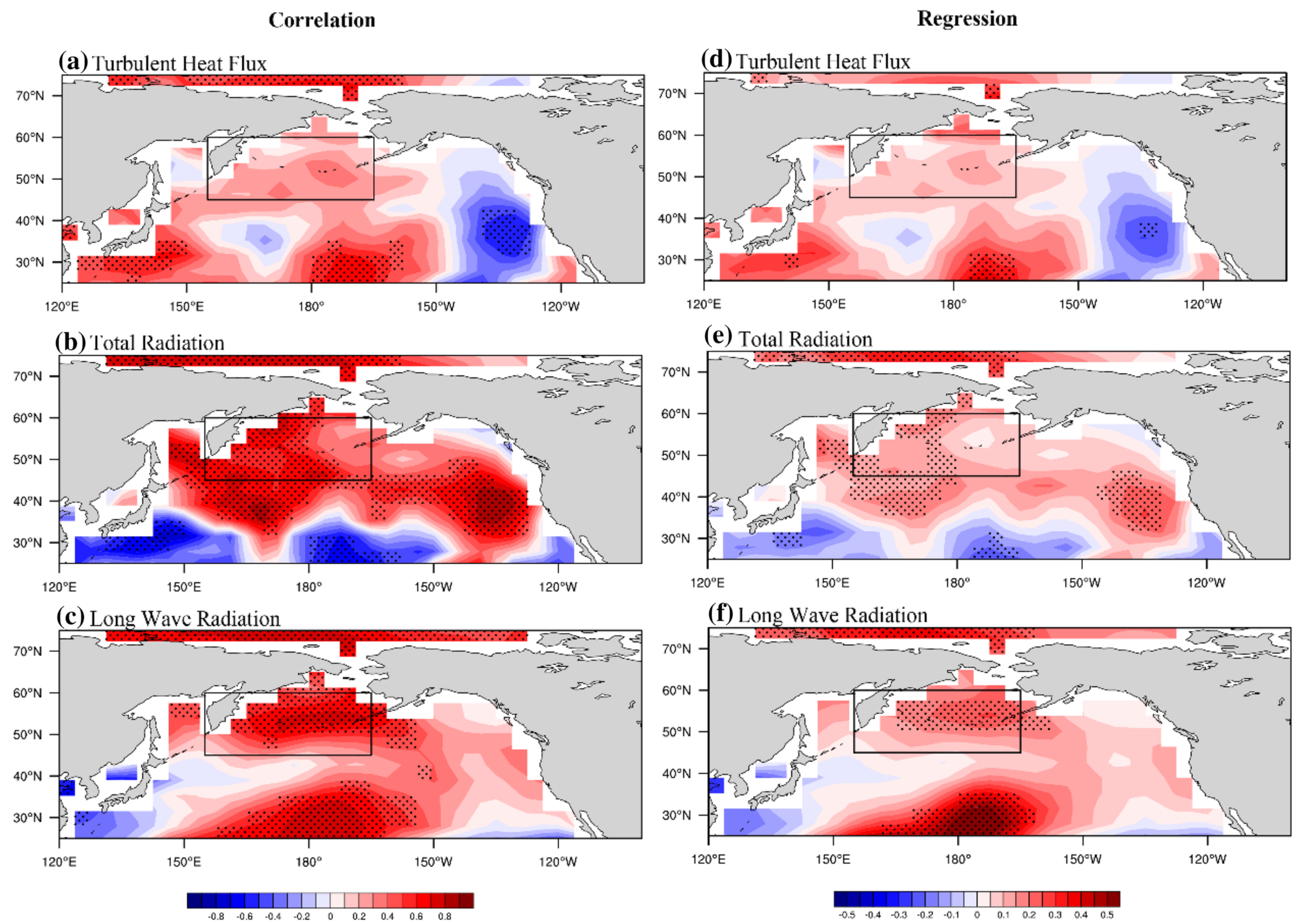

Fig. 5 The correlation maps of **a** surface turbulent heat flux (latent and sensible heat flux, W m^{-2}), **b** total radiation flux (longwave radiation and shortwave radiation) and **c** net surface longwave radiation anomalies with the normalized AMO index for 1900–2013 in the ATL_VARMIX experiment. The regression maps of **d** surface turbulent heat flux, **e** total radiation flux and **f** net surface longwave radiation anomalies onto the normalized AMO index for 1900–2013 in the ATL_VARMIX experiment. All fluxes anomalies are defined as positive downward, and dotted shading in **a**–**f** indicates the correlation and regression coefficients significant at the 99% confidence level. The long-term linear trends for 1900–2013 in all variables were removed before the correlation and regression analysis

through the lagged regressions (Fig. 6b). The turbulent heat flux anomalies still show a positive but weak regression result in response to the AMO. These results suggest that the AMO has an impact on the surface heat budget over the SANP region, especially the anomalous longwave radiation with a resultant SANP SST warming.

In the ATL_VARMIX experiment, the subarctic North Pacific air temperature (Fig. 7a) and water vapor (Fig. 7b) at 850 hPa show positive anomalies in response to the AMO forcing. It is well known that water vapor is the dominant greenhouse gas and absorbs longwave radiation. In addition, the simulated anomalies of net surface longwave radiation (LWR) are consistent with the observed anomalies of air temperature and water vapor at 850 hPa over the SANP region. Thus, these results indicate a water vapor (WV)-longwave radiation-SST positive feedback over the SANP region. The anomalous lower level water vapor increases, causing anomalous downwelling longwave radiation and preventing the loss of surface longwave radiation. Therefore, the increased longwave radiation anomalies result in SANP SST warming. The warm SST anomalies can warm up the low-level air temperature and further increase the content of water vapor, which reinforces the SST anomalies. Therefore, this process forms a WV-longwave radiation-SST positive feedback over the SANP region.

3.3 An atmospheric bridge mechanism

The above analyses indicate that the WV-longwave radiation-SST positive feedback plays an important role in the SANP SST decadal variability response to the AMO, but how the positive feedback is excited by the AMO needs to be further addressed. Consistent with the results presented above, there has also been some observational evidence.

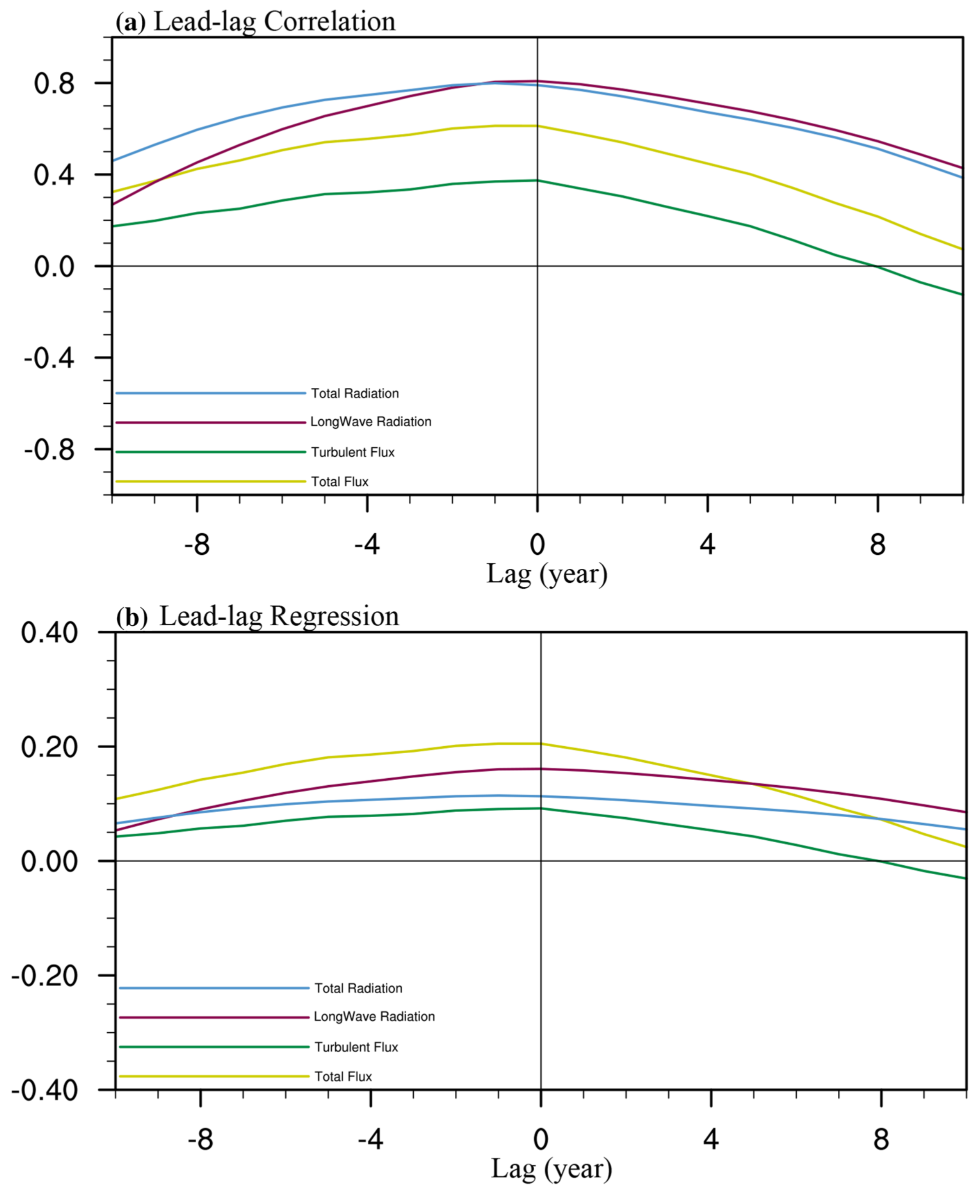

Fig. 6 **a** Lead–lag correlations of the surface total heat flux (the sum of the radiative and turbulent flux at the surface, W m^{-2}), surface turbulent heat flux (latent and sensible heat flux, W m^{-2}), net surface longwave radiation and total radiation flux (longwave radiation and shortwave radiation) anomalies over the SANP region onto the decadally filtered AMO index in the ATL_VARMIX experiment. Negative (positive) lags indicate the AMO leading (lagging) the fluxes. **b** As in **a**, but for lead–lag regressions (units: W m^{-2})

In response to the AMO forcing, the anomalous 200 hPa velocity potential over the North Atlantic and North Pacific basins shows a zonal dipole structure in both observational (Fig. 8a) and simulated results (Fig. 9a), with anomalous upper-level convergence over the North Pacific region and divergence over the North Atlantic, but significant over tropical region. The upper-level convergence induces compensating subsidence, further induces high pressure anomalies over the North Pacific basin (Figs. 8b, 9b), including both tropical Pacific and SANP regions. The anomalous 300 hPa geopotential height increases over the SANP region (Fig. 8b), accompanied by increased 850 hPa temperature anomalies (Fig. 8c) and water vapor anomalies (Fig. 8d). Both the velocity potential anomalies and the geopotential height anomalies are consistently strong in North Pacific and statistically significant in limited parts of the SANP region. These remote atmospheric responses can be physically interpreted.

During the AMO warm phase, warming SST anomalies lead to anomalous ascending motion, inducing upper-level divergence over the North Atlantic. The most strong and significant anomalous wind divergence appears at the tropical Atlantic while major convergence anomalies occur at the tropical Pacific (Fig. 8a). The anomalous upper-level divergence over the North Atlantic outflow heads westward and converges over the North Pacific, particularly significant in the tropical Pacific. This is in agreement with previous studies (Ruprich-Robert et al. 2017; McGregor et al. 2015; Sun et al. 2017) that demonstrated the tropical Atlantic SST role in modulating the Pacific climate, particularly the tropical Pacific. Over the extratropical regions, previous modeling studies have shown that the North Pacific atmospheric

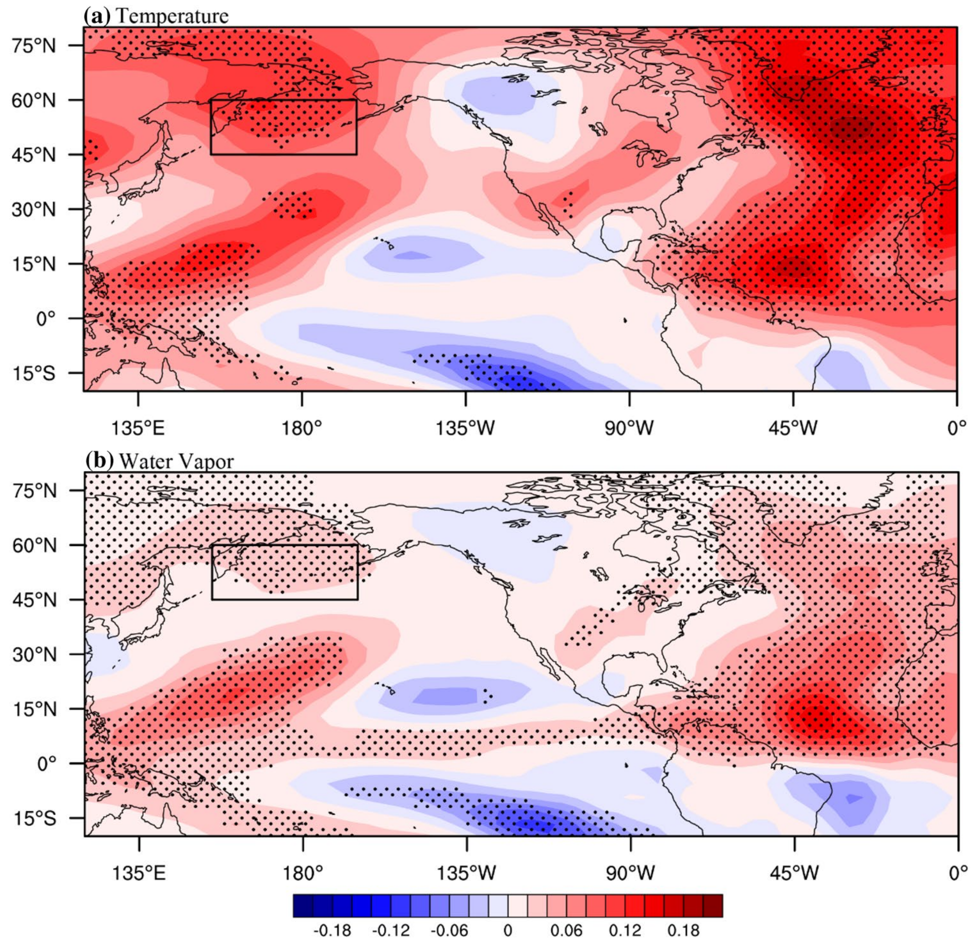

Fig. 7 **a** 850 hPa temperature anomalies (K) in response to the AMO forcing in the ATL_VAR-MIX experiment, shown as regression onto the normalized AMO index for 1900–2013. **b** As in **a**, but for the 850 hPa water vapor anomalies (g kg^{-1}). Dotted shading in **a** and **b** represents the regression coefficients significant at the 99% confidence level. The long-term linear trends for 1900–2013 in all variables were removed before the regression analysis

teleconnection pattern in response to the Atlantic warming (for both tropical and entire North Atlantic SST forcings) is characterized by an anomalous high in the SANP region (Zhang and Delworth 2007; Ruprich-Robert et al. 2017; McGregor et al. 2015; Sun et al. 2017). In this study, we focus on the association between the AMO and SANP region and find that in both observation and slab ocean model there is an anomalous high associated with the AMO SST warming (Figs. 8b, 9b). Thus, our finding of the atmospheric teleconnection associated with entire North Atlantic SST forcing (i.e., the AMO) is generally consistent with the previous modeling studies on the roles of tropical Atlantic (Ruprich-Robert et al. 2017; McGregor et al. 2015) and entire North Atlantic (Zhang and Delworth 2007).

The strong positive velocity potential and converging wind anomalies over the SANP region in response to the AMO at upper level are apparent, and this obvious SANP upper level anomalous convergence induces compensating subsidence, further induces an anomalous high over the SANP region. Thus, the atmospheric circulation and vertical velocity are strongly coupled, and the enhanced adiabatic descent associated with the high pressure anomalies contributes to the atmospheric warming occurring at lower troposphere (Fig. 8c) and changes in water vapor in response to the lower level warming (Fig. 8d). The increased water vapor anomaly is a direct result of lower level warming as indicated in the Clapeyron–Clausius equation and it further leads to increased downwelling longwave radiation above the SANP region. As we discussed above, longwave radiation role is also taken into consideration as it results in increasing and amplifying surface air temperature anomalies. This process is similar to the previous studies about relations among high-latitude atmospheric circulation, surface temperature and longwave radiation (Ding et al. 2017; Grunseich and Wang 2016). These studies examine the atmospheric circulation role in influencing the surface air temperature change over the high-latitude region. They pointed out that upper- and mid-level high anomalies and the adiabatic descent motion lead to lower-tropospheric warming and moistening, which further cause increases in downwelling longwave radiation and surface warming (Ding et al. 2017). Therefore, the anomalous upper level circulation and the associated lower-troposphere warming and moistening over the SANP region excites the WV-longwave radiation-SST positive feedback, which further warms up the SST and amplifies the warm anomalies.

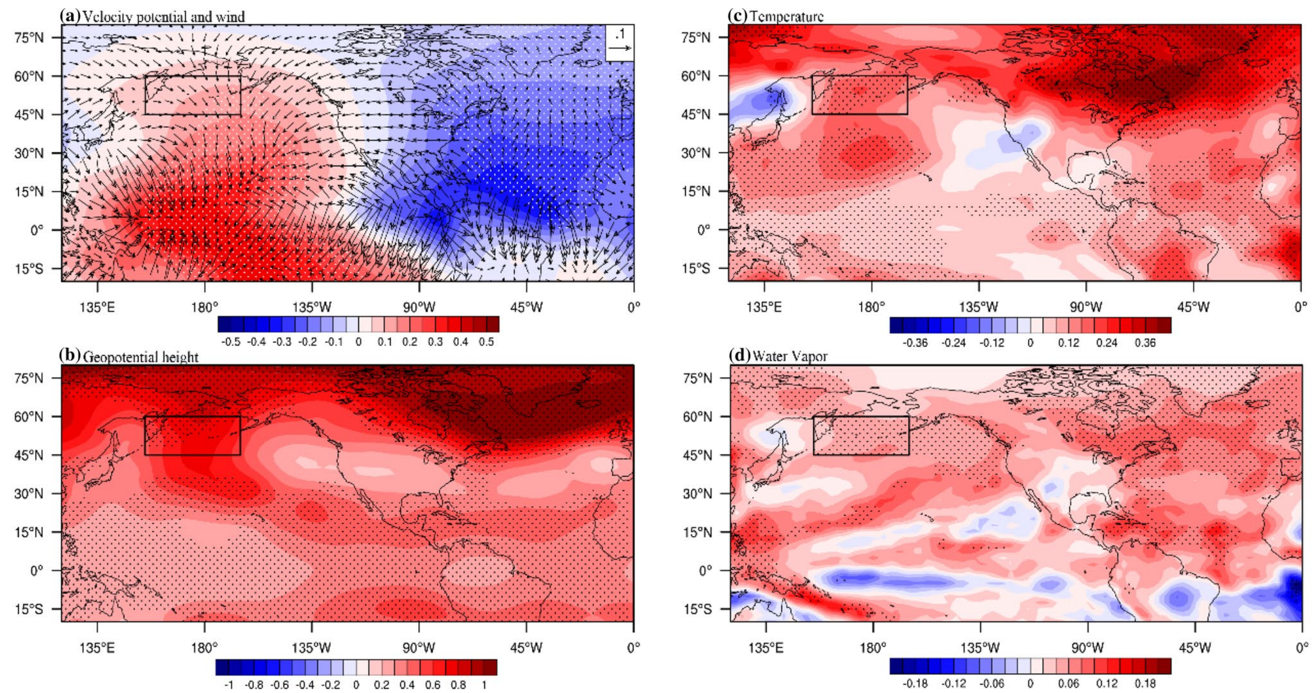

Fig. 8 **a** 200 hPa velocity potential (shading, units: 10^5 m^2 s^{-2}) and divergent wind (vectors, units: m s^{-1}; omitted below 0.1 m s^{-1}) anomalies in response to the AMO forcing in the observation, shown as regression onto the normalized AMO index at decadal time scales. **b** As in **a** but for the 300 hPa geopotential height (m). **c** As in **a** but for the 850 hPa temperature (K) anomalies. **d** As in **a**, but for the 850 hPa water vapor (g kg^{-1}) anomalies. Dotted shading in **a**–**d** represents the regression coefficients significant at the 99% confidence level. The long-term linear trends for 1900–2010 in all variables were removed before the regression analysis

In addition, the atmospheric mechanism between the AMO and the SANP SST decadal variability can be reproduced well in the ATL_VARMIX experiment (Fig. 9) despite of the regional differences, which further verifies that the AMO teleconnection to the SANP SST decadal variability is due to the WV-longwave radiation-SST positive feedback and the effect of turbulent heat flux. We can see that the atmospheric circulation elements associated with the AMO all show significant features over the SANP region, which may be the reason why the AMO teleconnection mainly takes place over the SANP region.

Figure 10 finally shows a schematic graph that identifies the physical mechanisms involved in the inter-basin teleconnection between the AMO and the SANP SST multidecadal variability. In summary, during the AMO warm phase, SST anomalies generate anomalous ascent and upper-level divergence over the North Atlantic. The associated upper-level outflows converge towards the subarctic North Pacific, leading to compensating subsidence along with an anomalous high pressure there, causing anomalous warming and moistening of the lower level due to the enhanced adiabatic descent, which further induces and amplifies the SANP SST warming through the WV-longwave radiation-SST positive feedback. In addition, the anomalous high also weakens the climatological cyclonic flow of Aleutian low and suppresses the turbulent heat release from ocean to atmosphere, contributing to the SANP SST warming.

4 Summary and discussion

The SST over the subarctic North Pacific (SANP; 45°–60° N, 155° E–165° W) region shows pronounced multidecadal variability in observational records, which cannot be explained by the PDO, though the PDO is the first leading mode of SST variability over the extratropical North Pacific basin. The observed SANP SST multidecadal variation follows the remote influence of the AMO signal, indicating the existence of an inter-basin teleconnection. This teleconnection can be well reproduced in a set of Atlantic Pacemaker simulations, and a heat budget analysis provides a positive feedback referred to the water vapor-longwave radiation-SST, which plays a crucial role at lower level in the SANP region. The AMO warm phase induces an atmospheric teleconnection into the SANP, resulting in warming and moistening of the lower troposphere, and further generates and amplifies the SANP SST warming via the water vapor-longwave radiation-SST positive feedback.

Previous modeling studies indicated that the teleconnection between the North Atlantic and the North Pacific

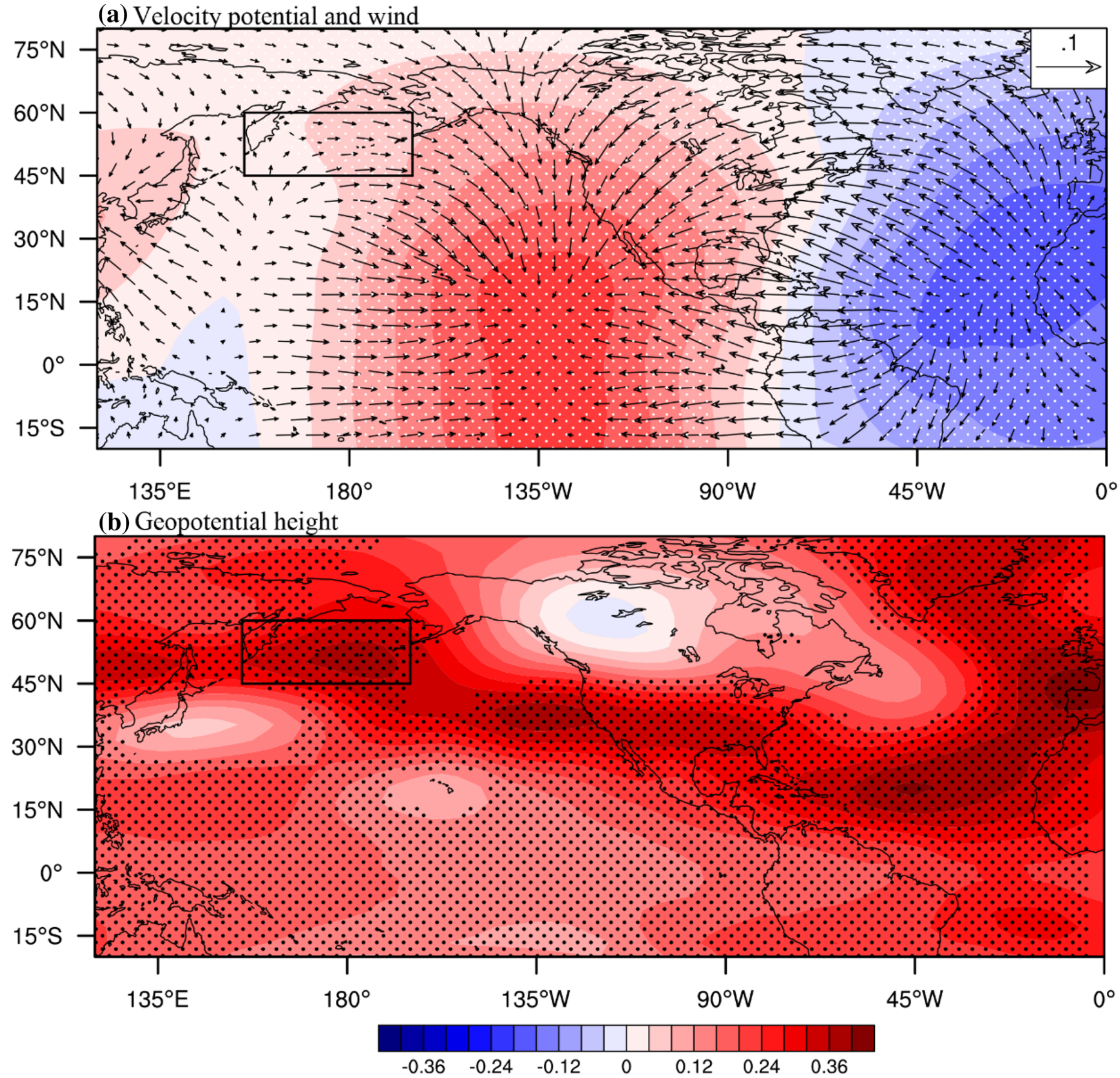

Fig. 9 **a** 100 hPa velocity potential (shading, units: 10^5 m^2 s^{-2}) and divergent wind (vectors, units: m s^{-1}; omitted below 0.1 m s^{-1}) anomalies in response to the AMO forcing in the ATL_VARMIX experiment, shown as regression onto the normalized AMO index for 1900–2010. **b** As in **a** but for the 300 hPa geopotential height (m) anomalies. Dotted shading in **a** and **b** represents the regression coefficients significant at the 99% confidence level. The long-term linear trends for 1900–2010 in all variables were removed before the regression analysis

is robust over the midlatitudes, and an atmospheric bridge mechanism was found responsible for this inter-basin multidecadal variability, with the Aleutian low acting as a key aspect of the North Pacific response to the Atlantic (Li et al. 2009; Okumura et al. 2009). Our results are consistent with their findings to some extent. In addition, our results indicate that in both the observations and the ATL_VARMIX experiment, the AMO teleconnections to the North Pacific SST and atmospheric circulation anomalies are most significantly robust over the SANP at decadal time scales. While from Figs. 1 and 4, we can see that over the midlatitude North Pacific, there is also a prominent warming response to the AMO along the west coast of North America in observations which cannot be found in the model results. These discrepancies may possibly be attributed to the role of ocean dynamics, which is important for the SST variability over Northeast Pacific (Chhak and Di Lorenzo 2007; Di Lorenzo et al. 2008). It should also be noted that though the SANP SST multidecadal variability and the AMO are highly correlated with more than 60% multidecadal variance explained, the AMO is not the only factor forcing the SANP SST multidecadal variability. We cannot rule out the possibility that other forcings (e.g., external forcings) may also play a role in the SANP SST multidecadal variability.

A number of studies have also proposed the oceanic bridge responsible for the inter-basin teleconnection

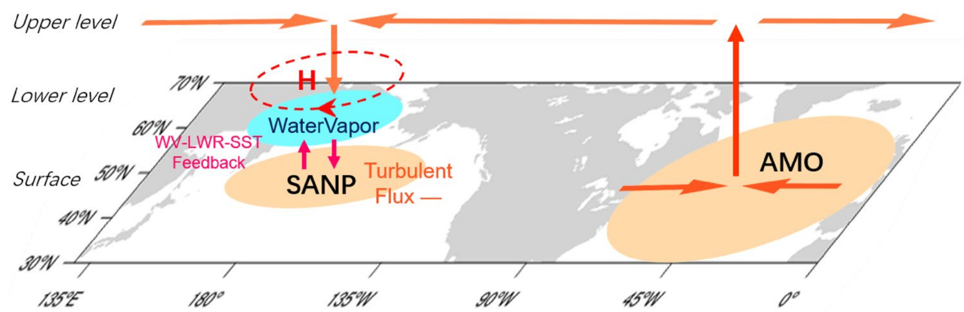

Fig. 10 Schematic representation of the mechanism of inter-basin connection between the AMO and the SANP SST multidecadal variability. In the AMO warm phase, the SST anomalies result in upper-level divergence over the North Atlantic. The associated upper-level outflows converge towards the subarctic North Pacific (orange patch in the North Pacific), leading to compensating subsidence along with an anomalous geopotential height there, causing anomalous warming and moistening of the lower level due to the enhanced adiabatic descent, which further induces and amplifies the SANP SST warming through the WV-longwave radiation-SST positive feedback. The anomalous high also weakens the climatological cyclonic flow of Aleutian low and suppresses the turbulent heat release from ocean to atmosphere (represented by Turbulent Flux –), contributing to the SANP SST warming

between the North Atlantic and the North Pacific through the Arctic Ocean (Okumura et al. 2009; Wu et al. 2008). Thus, further comparisons between the atmospheric bridge and the oceanic bridge by using fully coupled models are needed. On the other hand, there is observational evidence showing Arctic warming for 1920–1944 (Jones and Moberg 2003), when the climate was not significantly affected by anthropogenic activities. Some studies have indicated that the early twentieth century Arctic climate variability tends to be an internal variability and that Arctic temperature changes are significantly correlated with the AMO (Chylek et al. 2009; Tokinaga et al. 2017). We find that the subarctic North Pacific is mainly affected by the AMO. Further studies are needed to discuss the connection between the SANP and the Arctic region for a better understanding of the North Atlantic remote impacts over the North Pacific and hence the Arctic region.

Acknowledgements The authors wish to thank the anonymous reviewers for their constructive comments that significantly improved the quality of this paper. This work was jointly supported by the National Natural Science Foundation of China (41775038, 41975082, and 41790474), the National Program on Global Change and Air–Sea Interaction (GASI-IPOVAI-03 and GASI-IPOVAI-06) and the National Key Research and Development Plan (2016YFA0601801). C.S. is supported by the State Key Laboratory of Tropical Oceanography, South China Sea Institute of Oceanology, Chinese Academy of Sciences (Project LTO1801).

References

Bromirski PD, Miller AJ, Flick RE, Auad G (2011) Dynamical suppression of sea level rise along the Pacific coast of North America: indications for imminent acceleration. J Geophys Res 116:C07005. https://doi.org/10.1029/2010JC006759

Chhak K, Di Lorenzo E (2007) Decadal variations in the California Current upwelling cells. Geophys Res Lett 314:L14604. https://doi.org/10.1029/2007GL030203

Chylek P, Folland CK, Lesins G, Dubey MK, Wang M (2009) Arctic air temperature change amplification and the Atlantic Multidecadal Oscillation. Geophys Res Lett 36:L14801. https://doi.org/10.1029/2009GL038777

Clement AC, Burgman R, Norris JR (2009) Observational and model evidence for positive low-level cloud feedback. Science 325(5939):460–464

Danielson S, Curchitser E, Hedstrom K, Weingartner T, Stabeno P (2011) On ocean and sea ice modes of variability in the Bering Sea. J Geophys Res Oceans 116:24

Delworth TL, Mann ME (2000) Observed and simulated multidecadal variability in the Northern Hemisphere. Clim Dyn 16:661–676

Deser C, Alexander MA, Timlin MS (1999) Evidence for a wind-driven intensification of the Kuroshio current extension from the 1970s to the 1980s. J Clim 12:1697–1706

Di Lorenzo E, Schneider N, Cobb KM, Chhak K, Franks PJS, Miller AJ, McWilliams JC, Bograd SJ, Arango H, Curchister E, Powell TM, Rivere P (2008) North Pacific Gyre Oscillation links ocean climate and ecosystem change. Geophys Res Lett 35:L08607. https://doi.org/10.1029/2007GL032838

Ding QH, Schweiger A, L'Heureux M, Battisti DS, Po-Chedley S, Nathaniel CJ, Blanchard-Wrigglesworth E, Harnos K, Zhang Q, Eastman R, Steig EJ (2017) Influence of high-latitude atmospheric circulation changes on summertime Arctic sea ice. Nat Clim Change 7:289–295. https://doi.org/10.1038/NCLIMATE3241

d'Orgeville M, Peltier WR (2007) On the Pacific decadal oscillation and the Atlantic multidecadal oscillation: might they be related? Geophys Res Lett 34(23):L23705. https://doi.org/10.1029/2007GL031584

Enfield DB, Cid-Serrano L (2009) Secular and multidecadal warmings in the North Atlantic and their relationships with major hurricane activity. Int J Climatol 30:174–184

Enfield DB, Mestas-Nuñez AM, Trimble PJ (2001) The Atlantic multidecadal oscillation and its relation to rainfall and river flows in the continental US. Geophys Res Lett 28:2077–2080

Folland CK, Rayner NA, Brown SJ, Smith TM, Shen SSP, Parker DE, Macadam I, Jones PD, Jones RN, Nicholls N, Sexton DMH (2001) Global temperature change and its uncertainties since 1861. Geophys Res Lett 28:2621–2624

Frankcombe LM, England MH (2018) On the choice of ensemble mean for estimating the forced signal in the presence of internal variability. J Clim 31:5681–5693
Frankcombe LM, England MH, Mann ME, Steinman BA (2015) Separating internal variability from the externally forced climate response. J Clim 28(20):8184–8202. https://doi.org/10.1175/JCLI-D-15-0069.1
Grunseich G, Wang B (2016) Arctic sea ice patterns driven by the Asian summer monsoon. J Clim 29:9097–9112
Hartmann B, Wendler G (2005) The significance of the 1976 Pacific climate shift in the climatology of Alaska. J Clim 18:4824–4839
Hetzinger S, Halfar J, Mecking JV, Keenlyside NS, Kronz A, Steneck RS, Adey WH, Lebednik PA (2011) Marine proxy evidence linking decadal North Pacific and Atlantic climate. Clim Dyn 39:1447–1455
Hu AX, Meehl GA (2005) Bering Strait throughflow, and the thermohaline circulation. Geophys Res Lett 32:L24610. https://doi.org/10.1029/2005GL024424
Hunt GL, Stabeno P, Walters G, Sinclair E, Brodeur RD, Napp JM, Bond NA (2002) Climate change and control of the southeastern Bering Sea pelagic ecosystem. Deep Sea Res Part II Top Stud Oceanogr 49:5821–5853
Hunt GL, Coyle KO, Eisner LB, Farley EV, Heintz RA, Mueter F, Napp JM, Overland JE, Ressler PH, Salo S, Stabeno PJ (2011) Climate impacts on eastern Bering Sea foodwebs: a synthesis of new data and an assessment of the Oscillating Control Hypothesis. ICES J Mar Sci 68:1230–1243
Ishii M, Shouji A, Sugimoto S, Matsumoto T (2005) Objective analyses of sea-surface temperature and marine meteorological variables for the 20th century using ICOADS and the Kobe collection. Int J Climatol 25:865–879
Jones PD, Moberg A (2003) Hemispheric and large-scale surface air temperature variations: an extensive revision and an update to 2001. J Clim 16:206–223
Kaplan A, Cane MA, Kushnir Y, Clement AC, Blumenthal MB, Rajagopalan B (1998) Analyses of global sea surface temperature 1856–1991. J Geophys Res Oceans 103:18567–18589
Kerr RA (2000) A North Atlantic climate pacemaker for the centuries. Science 288:1984–1986
Knight JR, Allan RJ, Folland CK, Vellinga M, Mann ME (2005) A signature of persistent natural thermohaline circulation cycles in observed climate. Geophys Res Lett 32:L20708. https://doi.org/10.1029/2005GL024233
Kosaka Y, Xie S-P (2013) Recent global-warming hiatus tied to equatorial Pacific surface cooling. Nature 501(7467):403–407. https://doi.org/10.1038/nature12534
Kucharski F, Parvin A, Rodriguez-Fonseca B, Farneti R, Martin-Rey M, Polo I, Mohino E, Losada T, Mechoso CR (2016) The teleconnection of the tropical Atlantic to Indo-Pacific sea surface temperatures on inter-annual to centennial time scales: a review of recent findings. Atmosphere 7:29
Kushnir Y, Robinson WA, Bladé I, Hall NMJ, Peng S, Sutton R (2002) Atmospheric GCM response to extratropical SST anomalies: synthesis and evaluation. J Clim 15:2233–2256
Li S, Bates GT (2007) Influence of the Atlantic multidecadal oscillation on the winter climate of East China. Adv Atmos Sci 24:126–135
Li C, Wu L, Wang Q, Qu L, Zhang L (2009) An intimate coupling of ocean–atmospheric interaction over the extratropical North Atlantic and Pacific. Clim Dyn 32:753–765
Li J, Sun C, Jin FF (2013) NAO implicated as a predictor of Northern Hemisphere mean temperature multidecadal variability. Geophys Res Lett 40:5497–5502
Li XC, Xie SP, Gille ST, Yoo C (2015) Atlantic-induced pan-tropical climate change over the past three decades. Nat Clim Change 6:275–279
Liu Z, Alexander M (2007) Atmospheric bridge, oceanic tunnel, and global climatic teleconnections. Rev Geophys 45:RG2005. https://doi.org/10.1029/2005RG000172
Lopez H, Dong SF, Lee SK, Goni G (2016) Decadal modulations of interhemispheric global atmospheric circulations and monsoons by the South Atlantic meridional overturning circulation. J Clim 29:1831–1851
Lu R, Dong B, Ding H (2006) Impact of the Atlantic multidecadal oscillation on the Asian summer monsoon. Geophys Res Lett 33(24):L24701. https://doi.org/10.1029/2006GL027655
Lyu K, Yu JY (2017) Climate impacts of the Atlantic Multidecadal Oscillation simulated in the CMIP5 models: a re-evaluation based on a revised index. Geophys Res Lett 44:3867–3876
Mantua NJ, Hare SR, Zhang Y, Wallace JM, Francis RC (1997) A Pacific interdecadal climate oscillation with Impacts on Salmon Production*. Bull Am Meteorol Soc 78:1069–1080
McCabe GJ, Palecki MA, Betancourt JL (2004) Pacific and Atlantic Ocean influences on multidecadal drought frequency in the United States. Proc Natl Acad Sci USA 101:4136–4141
McGregor S, Timmermann A, Stuecker MF, England MH, Merrifield M, Jin FF, Chikamoto Y (2014) Recent Walker circulation strengthening and Pacific cooling amplified by Atlantic warming. Nat Clim Change 4:888–892
McGregor HV, Evans MN, Goosse H, Leduc G, Martrat B, Addison JA, Mortyn PG, Oppo DW, Seidenkrantz M-S, Sicre M-A, Phipps SJ, Selvaraj K, Thirumalai K, Filipsson HL, Ersek V (2015) Robust global ocean cooling trend for the pre-industrial Common Era. Nature Geosci 8:671–677. https://doi.org/10.1038/ngeo2510
Mueter FJ, Litzow MA (2008) Sea ice retreat alters the biogeography of the Bering Sea continental shelf. Ecol Appl 18:309–320
Okumura YM, Deser C, Hu A, Timmermann A, Xie S-P (2009) North Pacific climate response to freshwater forcing in the subarctic North Atlantic: oceanic and atmospheric pathways. J Clim 22:1424–1445
O'Reilly CH, Woollings T, Zanna L (2017) The dynamical influence of the Atlantic multidecadal oscillation on continental climate. J Clim 30:7213–7230
Peings Y, Magnusdottir G (2016) Wintertime atmospheric response to Atlantic multidecadal variability: effect of stratospheric representation and ocean–atmosphere coupling. Clim Dyn 47:1029–1047
Rayner NA, Parker DE, Horton EB, Folland CK, Alexander LV, Rowell DP, Kent EC, Kaplan A (2003) Global analyses of sea surface temperature, sea ice, and night marine air temperature since the late nineteenth century. J Geophys Res. https://doi.org/10.1029/2002JD002670
Richter I, Xie SP, Behera SK, Doi T, Masumoto Y (2014) Equatorial Atlantic variability and its relation to mean state biases in CMIP5. Clim Dyn 42:171–188
Ruprich-Robert Y, Msadek R, Castruccio F, Yeager S, Delworth T, Danabasoglu G (2017) Assessing the climate impacts of the observed AMV using the GFDL CM2.1 and NCAR CESM1 global coupled models. J Clim 30:2785–2810
Schlesinger ME, Ramankutty N (1994) An oscillation in the global climate system of period 65–70 years. Nat Clim Change 367:723–726
Smith TM, Reynolds RW, Peterson TC, Lawrimore J (2008) Improvements to NOAA's historical merged land–ocean surface temperature analysis (1880–2006). J Clim 21:2283–2296
Stabeno PJ, Kachel NB, Moore SE, Napp JM, Sigler M, Yamaguchi A, Zerbini AN (2012) Comparison of warm and cold years on the southeastern Bering Sea shelf and some implications for the ecosystem. Deep Sea Res Part II Top Stud Oceanogr 65:31–45
Stickler A, Brönnimann S, Valente MA, Bethke J, Sterin A, Jourdain S, Roucaute E, Vasquez MV, Reyes DA, Allan R, Dee D (2014) ERA-CLIM: historical surface and upper-air data for future reanalyses. Bull Am Meteorol Soc 95(9):1419–1430

Stouffer RJ, Yin J, Gregory JM, Dixon KW, Spelman MJ, Hurlin W, Weaver AJ, Eby M, Flato GM, Hasumi H, Hu A, Jungclaus JH, Kamenkovich IV, Levermann A, Montoya M, Murakami S, Nawrath S, Oka A, Peltier WR, Robitaille DY, Sokolov A, Vettoretti G, Weber SL (2006) Investigating the causes of the response of the thermohaline circulation to past and future climate changes. J Clim 19:1365–1387

Sun C, Li J, Zhao S (2015) Remote influence of Atlantic multidecadal variability on Siberian warm season precipitation. Sci Rep 5:16853

Sun C, Li J, Ding R, Jin Z (2016) Cold season Africa–Asia multidecadal teleconnection pattern and its relation to the Atlantic multidecadal variability. Clim Dyn 48:3903–3918

Sun C, Kucharski F, Li J, Jin FF, Kang IS, Ding R (2017) Western tropical Pacific multidecadal variability forced by the Atlantic multidecadal oscillation. Nat Commun 8:15998

Sutton RT, Dong B (2012) Atlantic Ocean influence on a shift in European climate in the 1990s. Nat Geosci 5:788–792

Sutton RT, Hodson DLR (2005) Atlantic Ocean forcing of North American and European summer climate. Science 309:115–118

Timmermann A, Latif M, Voss R, Grotzner A (1998) Northern hemisphere interdecadal variability: a coupled air–sea mode. J Clim 11:1906–1931

Timmermann A, Okumura Y, An S-I, Clement A, Dong B, Guilyardi E, Hu A, Jungclaus JH, Renold M, Stocker TF, Stouffer RJ, Sutton R, Xie S-P, Yin J (2007) The influence of a weakening of the Atlantic meridional overturning circulation on ENSO. J Clim 20:4899–4919

Tokinaga H, Xie SP, Mukougawa H (2017) Early 20th-century Arctic warming intensified by Pacific and Atlantic multidecadal variability. Proc Natl Acad Sci USA 114:6227–6232

Trenberth KE, Fasullo JT (2013) An apparent hiatus in global warming? Earth's Future 1(1):19–32. https://doi.org/10.1002/2013EF000165

Trenberth KE, Shea DJ (2006) Atlantic hurricanes and natural variability in 2005. Geophys Res Lett 33:L12704

Wu L, Li C, Yang C, Xie S-P (2008) Global teleconnections in response to a shutdown of the Atlantic meridional overturning circulation. J Clim 21:3002–3019

Wu S, Liu Z, Zhang R, Delworth TL (2011) On the observed relationship between the Pacific Decadal Oscillation and the Atlantic Multi-decadal Oscillation. J Oceanogr 67:27–35

Zhang L (2016) The roles of external forcing and natural variability in global warming hiatuses. Clim Dyn 47(9–10):3157–3169. https://doi.org/10.1007/s00382-016-3018-6

Zhang R, Delworth TL (2007) Impact of the Atlantic multidecadal oscillation on North Pacific climate variability. Geophys Res Lett 34:L23708. https://doi.org/10.1029/2007GL031601

Zhang L, Wang C (2013) Multidecadal North Atlantic sea surface temperature and Atlantic meridional overturning circulation variability in CMIP5 historical simulations. J Geophys Res 118:5772–5791

Zhang Y, Wallace JM, Battisti DS (1997) ENSO-like interdecadal variability: 1900–1993. J Clim 10:1004–1020

Zhang R, Delworth TL, Sutton R, Hodson DLR, Dixon KW, Held IM, Kushnir Y, Marshall J, Ming Y, Msadek R, Robson J, Rosati AJ, Ting M, Vecchi GA (2013) Have aerosols caused the observed Atlantic multidecadal variability? J Atmos Sci 70:1135–1144